

Supporting Information

for *Adv. Funct. Mater.*, DOI: 10.1002/adfm.202205778

Origin of Lithiophilicity of Lithium Garnets: Compositing
or Cleaning?

*Hongpeng Zheng, Guoyao Li, Runxin Ouyang, Yao Han,
Hong Zhu, Yongmin Wu, Xiao Huang, Hezhou Liu, and
Huanan Duan**

Supporting Information

Origin of lithiophilicity of lithium garnets: compositing or cleaning?

Hongpeng Zheng^a, Guoyao Li^a, Runxin Ouyang^b, Yao Han^c, Hong Zhu^b, Yongmin Wu^d, Xiao Huang^e, Hezhou Liu^a, Huanan Duan^{a}*

^aH. Zheng, G. Li, H. Liu, H. Duan *

State Key Laboratory of Metal Matrix Composites, School of Materials Science and Engineering, Shanghai Jiao Tong University, Shanghai 200240, P. R. China

^bR. Ouyang, H. Zhu

University of Michigan-Shanghai Jiao Tong University Joint Institute, Shanghai Jiao Tong University, Shanghai 200240, China

^c Y. Han

Instrumental Analysis Center of SJTU, Shanghai Jiao Tong University, Shanghai 200240, P. R. China

^dY. Wu

State Key Laboratory of Space Power Technology, Shanghai Institute of Space Power-Sources, Shanghai 200245, P.R. China

^eX. Huang

SZU-NUS Collaborative Innovation Center for Optoelectronic Science & Technology, International Collaborative Laboratory of 2D Materials for Optoelectronics Science and Technology of Ministry of Education, Institute of Microscale Optoelectronics, Shenzhen University, Shenzhen 518060, P. R. China

Corresponding Author

*E-mail: hd1@sjtu.edu.cn

METHODS

Synthesis of garnet-type electrolyte and LLZTO powders

The cubic garnet $\text{Li}_{6.5}\text{La}_3\text{Zr}_{1.5}\text{Ta}_{0.5}\text{O}_{12}$ (LLZTO) was prepared by a conventional solid-state reaction method. Stoichiometric amounts of Li_2CO_3 , La_2O_3 , ZrO_2 , Ta_2O_5 were ball-milled in isopropanol for 24 h at 175 r min^{-1} . 20 wt% Li_2CO_3 was added to compensate for the lithium volatilization at high-temperature sintering. The mixed powder suspension was dried for 5 hours and calcined at $900 \text{ }^\circ\text{C}$ for 6 hours in air at $10 \text{ }^\circ\text{C min}^{-1}$. The calcined powders were ball-milled and dried for 5 h. The powders were sieved with 200 mesh sieves and were named the mother powder. Subsequently, the mother powders were pressed into pellets with a diameter of 12 mm under the pressure of 500 MPa; then, the green pellets were sintered at $1250 \text{ }^\circ\text{C}$ for 16 h covered with the same mother powders at $10 \text{ }^\circ\text{C min}^{-1}$ in the Al_2O_3 crucible. The prepared pellets were polished with 200, 500, 1000, and 2000-grit sandpapers to produce clean and flat surfaces. The pellets were transferred to the glovebox to avoid air contamination. LLZTO powders were ground with high-energy ball-milling at 1000 rpm for 12 h by a Frisch planetary ball milling. It paused for 3 minutes after every 3 minutes of grinding.

Synthesis of the anode foils and samples for XPS

The Li-C composite anode was synthesized by adding 20 wt % graphite powder into the molten Lithium, stirring for 10 min, cooling, and transferring into an aluminum-plastic film. The aluminum-plastic film was vacuumed and heat sealed. Li-C composite anode with a thickness of $70 \text{ }\mu\text{m}$ was obtained by physical rolling. The Li-LLZTO composite anode and the pure Li anode were prepared similarly.

Computational methods and models

All first-principle calculations were performed in the Vienna *ab-initio* Simulation Package (VASP)^[1], based on the density functional theory^[1] with the projector augmented wave method^[2] and generalized gradient approximation (GGA)

in the form of Perdew–Burke–Ernzerh of (PBE) exchange functional. The plane-wave energy cutoff of 500 eV was adopted. The convergence criterion of energy and force for calculations were 10^{-5} eV/atom and 0.01 eV \AA^{-1} , respectively. $1\times 1\times 1$, $7\times 7\times 7$, $7\times 7\times 7,5\times 5\times 5$ and $3\times 3\times 2$ Monkhorst–Pack^[3] k -meshes were applied for the Brillouin zone sampling of bulk $\text{Li}_{6.5}\text{La}_3\text{Zr}_{1.5}\text{Ta}_{0.5}\text{O}_{12}$ (LLZTO), Li, LiOH, LiF, Li_2CO_3 , Li_2O and LiC_6 , respectively. For the interface calculations, we applied a $1\times 1\times 1k$ -mesh.

The LLZTO (001)/LiOH (010), LLZTO (001)/LiF (001), LLZTO (001)/ Li_2CO_3 (001), LLZTO (001)/ LiC_6 (110) and LLZTO (001)/ Li_2O (001) interface models were constructed by matching the LLZTO (001) slab to Li_2CO_3 (001) slab, LiOH (010) slab, LiF(001) slab, Li(001)slab, LiC_6 (001) slab or Li_2O (001) slab, respectively, which are all the low-energy surfaces.^[4] Considering the high computation cost and the necessity for smaller interface mismatch, we have strained Li(001) 4×4 , LiOH (010) 3×4 and LiF(001) 3×3 , LiC_6 (110) 4×2 , Li_2CO_3 (001) 3×3 , Li_2O (001) 3×3 surface to match the Ta doped- $\text{Li}_7\text{La}_3\text{Zr}_2\text{O}_{12}$ (001) surface, and all the interface mismatch is showing in the Table S1.

Cell assembly and testing

Li/LLZTO/Li and Li-C/LLZTO/Li-C symmetric cells were assembled by the same methods as reported previously.^[5] The lithium plating/stripping test was carried out by galvanostatic cycling with a LAND CT2001A cell test system at 0.5 mA cm^{-2} at 35 °C. The electrochemical impedance spectroscopy (EIS) was recorded with the Solartron 1260 in the frequency range from 13 MHz to 1 Hz with a 10 mV amplitude. The distribution of relaxation times (DRT) was calculated by the free software of DRTtools as reported previously.^[6] All the parameters are consistent in the calculation process to ensure the consistency of the DRT results. For Li/LLZTO/LFP (LiFePO_4) full cell, the LFP cathode was prepared as reported previously.^[7] Briefly, LFP (80 wt.%), super P (10 wt.%) and PVDF (10 wt.%) was mixed in NMP solvent and cast onto an aluminum foil with active species loading of about 3.0 mg cm^{-2} . A small amount of liquid electrolyte (~ 15 μL , 1 M LiTFSI in a mixture of EC and DMC (volume ratio 1:1)) was added to wet the interface between cathode and LLZTO. The

cathode of NMC ($\text{LiNi}_{0.8}\text{Co}_{0.1}\text{Mn}_{0.1}\text{O}_2$) was prepared in the same way as the LFP. For Li/LLZTO/Sulfur cell, the cathode was prepared by grinding sulfur and Ketjen black (mass ratio 1:1) and heated at 175 °C for 6 hours. Then the KB-S (80 wt.%), super P (10 wt.%) and PVDF (10 wt.%) was mixed in an NMP solvent. The mixture was cast onto an Al foil and heated at 65 °C overnight to obtain the cathode. For Li/LLZTO/Sulfur cell, ~15 μL liquid electrolyte, 1 M LiTFSI in a mixture of DME and DOL (volume ratio 1:1) was added to wet the cathode interface. All the full cells were assembled in CR2032 cells. The electrode information and test conditions are listed in Table S4.

Materials characterization

Scanning electron microscopy (SEM) images were taken on a TESCAN Mira3 field emission scanning electron microscope (FESEM) attached with an energy dispersive spectroscopy (EDX). X-ray photoelectron spectroscopy (XPS) was performed using a Kratos Axis UltraDLD spectroscopy (Kratos Analytical-Ashimadzu Group Company) with monochromatic Al $K\alpha$ source (1486.6 eV). The power of the X-ray source was 100 W. The analysis area was $300 \times 700 \mu\text{m}$, and the analysis chamber pressure was less than 5×10^{-9} torr. The different depth composition of anode was characterized by XPS depth profile measurement using Ar^+ to sputter for different durations (100 s, 1500 s, 3000s and 3600 s) with an accelerating voltages of 2 KV. The sputtering area was $4 \times 4 \text{ mm}$ with current of 20 μA . Pass energies of 160 eV and 40 eV were used for the survey spectra and the detail spectra, respectively. In order to avoid the influence of the surrounding environment, the samples were transferred via a gastight container with the protection of Ar gas. The binding energy was calibrated according to the C 1s peak (284.8 eV) of adventitious carbon on the analyzed sample surface. Data evaluation was carried out with the software CasaXPS (version 2.3.23, Casa Software Ltd). The crystallographic phase was characterized by X-ray diffraction (XRD, D/MAX255ovl/84, Rigaku, Japan) using copper $K\alpha$ radiation. The powders were scanned from the $2\theta=15^\circ$ - 135° with a step size of 0.02° . Time-of-flight secondary ion mass spectrometry (TOF-SIMS) and TOF-SEM were carried out on a TESCAN Gaia3 FESEM attached with a TOF SIMS 5-100 instrument (ION TOF).

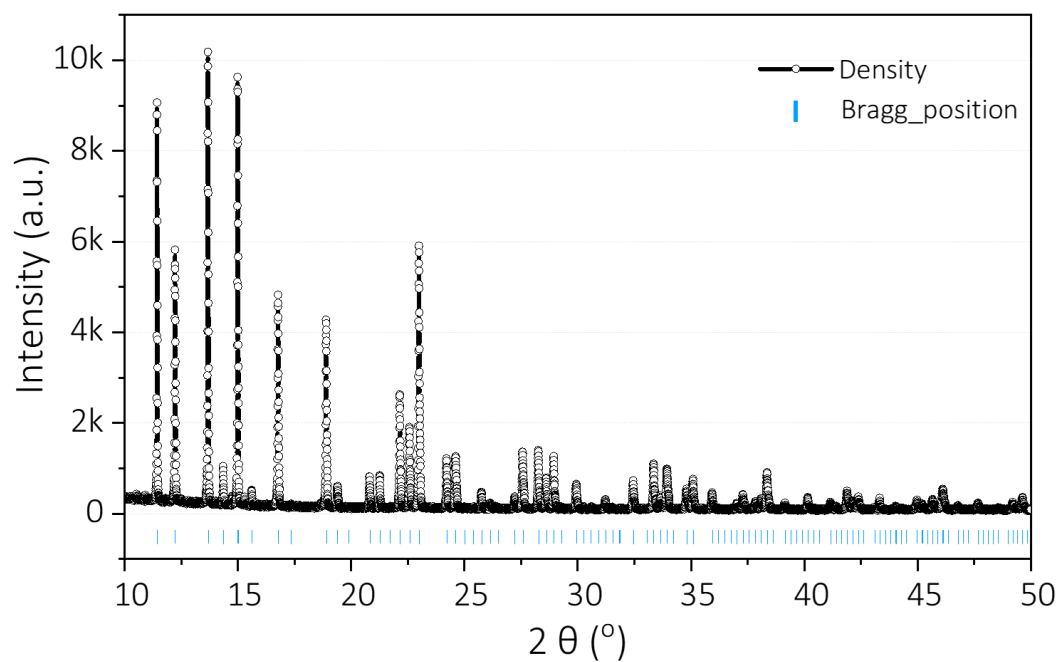


Figure S1 Powder XRD pattern of LLZTO electrolyte, measured by BL14B1

beamline at SSRF



Figure S2 Photograph of the molten lithium foil in the glovebox.

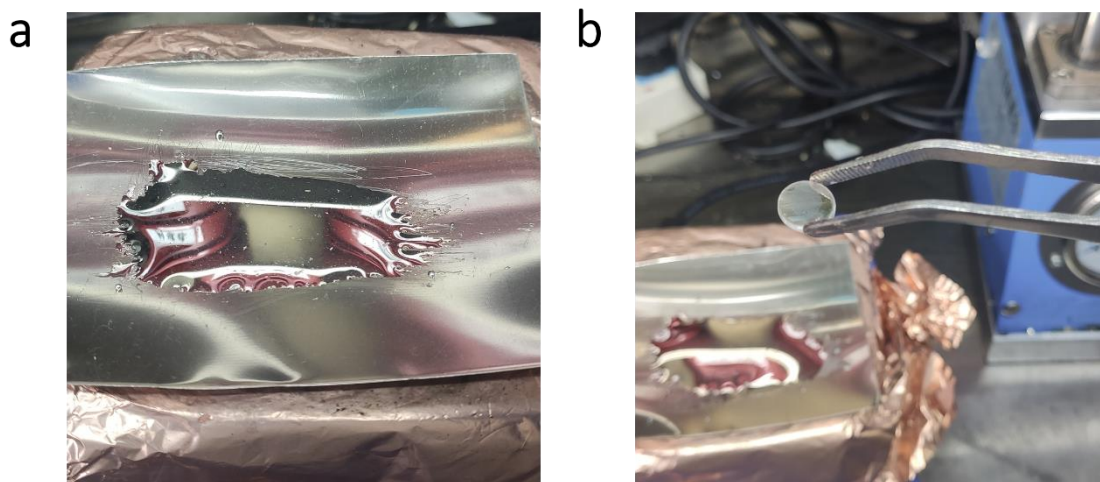


Figure S3 Photographs of the spread-Li (a) and the Li-wet LLZTO (b).

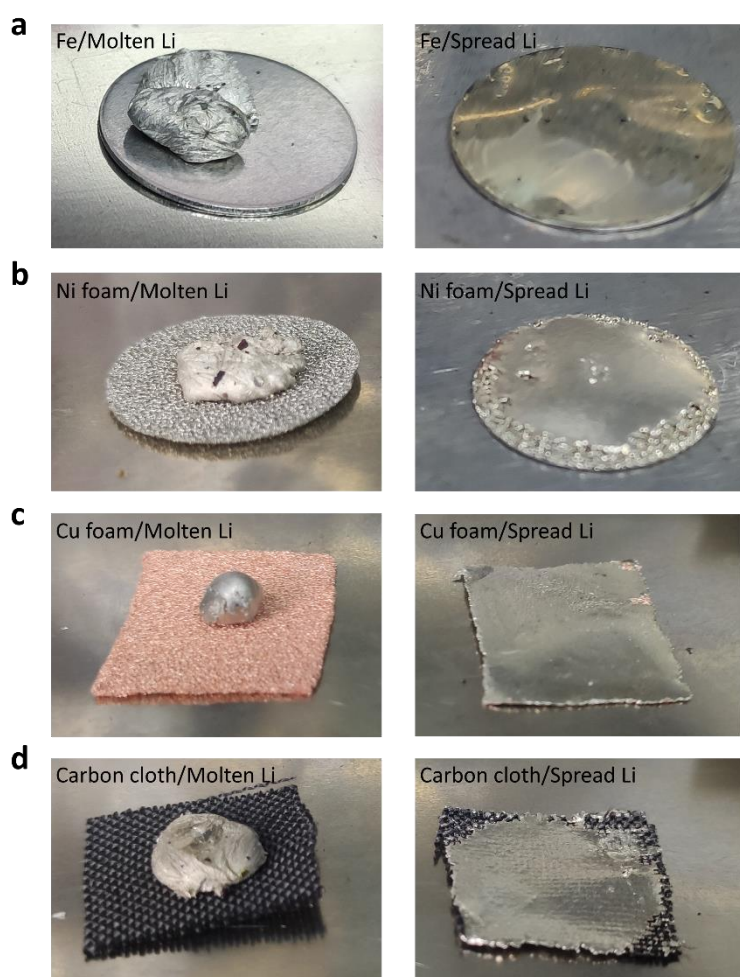


Figure S4 Photographs of the wetting behavior of molten and spread molten Li on different surfaces, Fe (a), Ni foam (b), Cu foam (c), and carbon cloth (d).

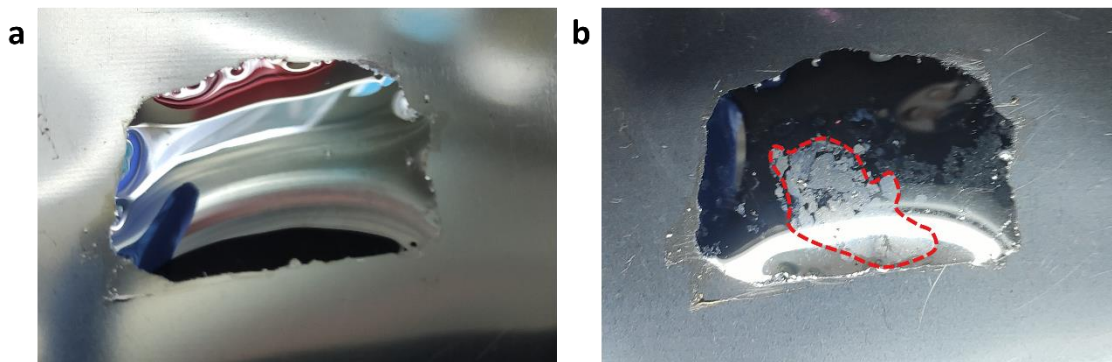


Figure S5 Photographs of the spread Li before (a) and after (b) contacting with the LLZTO polished in the air.

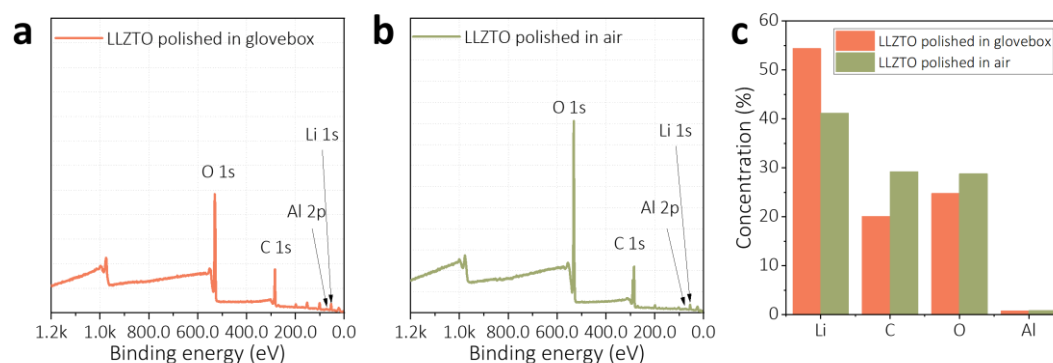


Figure S6 XPS survey of LLZTO polished in glovebox (a) and LLZTO polished in air (b). (c) Li, C, O and Al atoms ratios for LLZTO polished in glovebox and air.

Figure S6 shows the XPS characterization for LLZTO surface after polished in air and glovebox. We focus on the Li, C, O and Al elements on the LLZTO surface. Its corresponding binding energy are 55.0 eV (Li 1s, mainly from LLZTO), 284.32 eV (C 1s), 531.3 eV (O 1s) and 75.4 eV (Al 2P), respectively. Al is mainly derived from corundum in sandpaper, which is mainly used as abrasive. In Figure S6a, the LLZTO polished in the glovebox is mainly composed of Li (54.36 at%), C (20.09%), O (24.76%) and Al (0.79%), while the LLZTO polished in air composed of Li (41.18%), C (29.18%), O (28.8%) and Al (0.83%). Obviously, the C and O contents are smaller

in the LLZTO polished in the glovebox than those polished in air, which implies more impurity (e.g. Li_2CO_3 , adsorbed CO_2 and H_2O) on the LLZTO polished in air than that polished in glovebox. Subsequently, after contacting with the air-polished pellets, more impurities will form on the surface of molten lithium.



Figure S7 Photographs of the gastight container for XPS measurements.

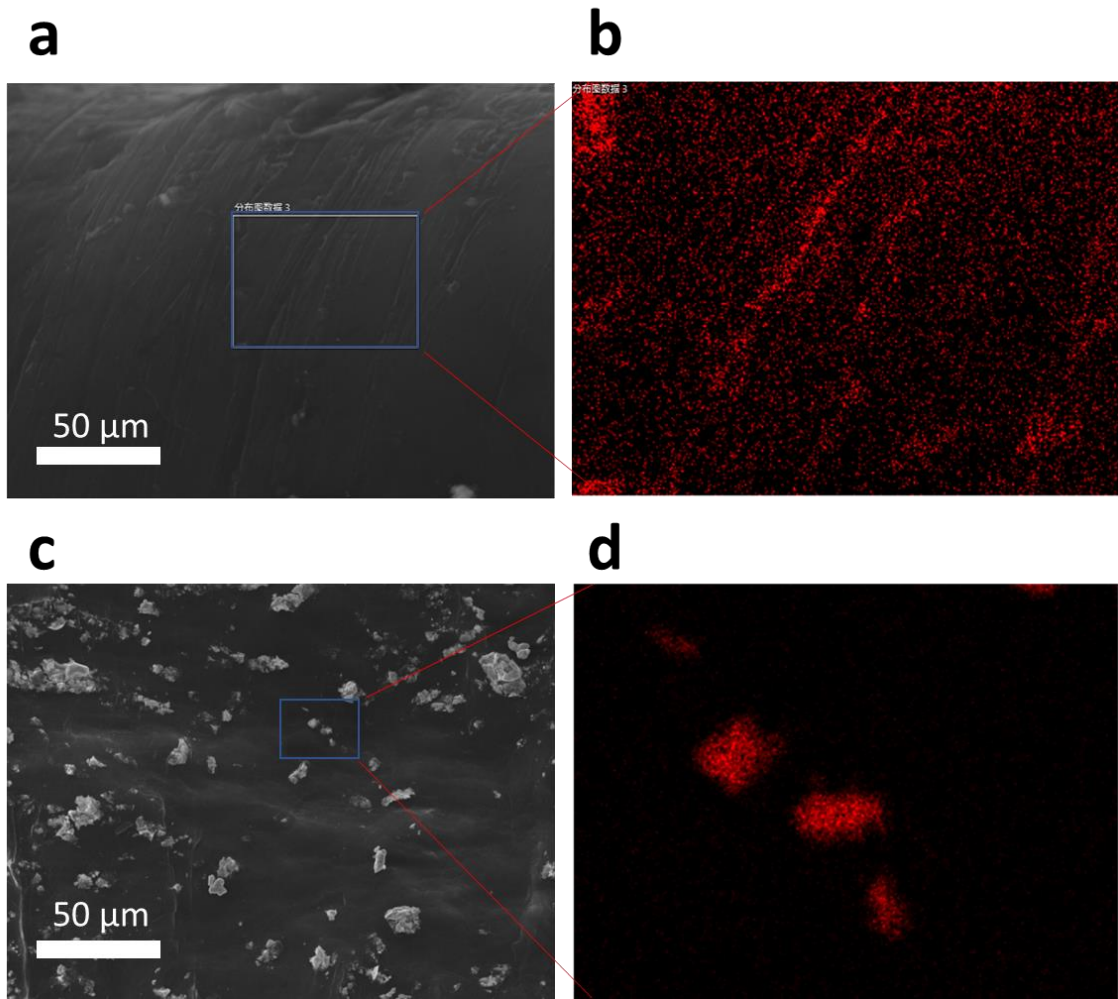


Figure S8 The cross-sectional SEM images of the Li-C (a) and Li-LLZTO (c) composite anode, and the corresponding EDX mapping for C and Zr in the Li-C (b) and the Li-LLZTO composite (d), respectively.

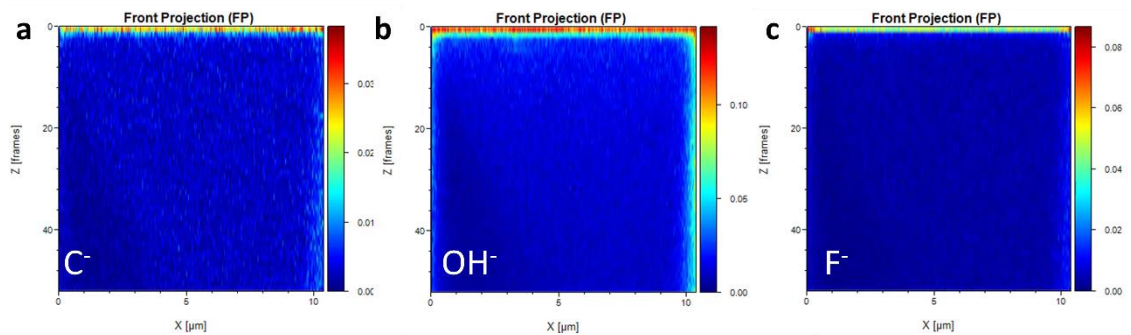


Figure S9 TOF-SIMS depth analysis of the C^- (Li_2CO_3) (a), OH^- ($LiOH$) (b), and F^- (LiF) (c) secondary ion (SI) signals to demonstrate the relatively thin impurity layer on the lithium surface.

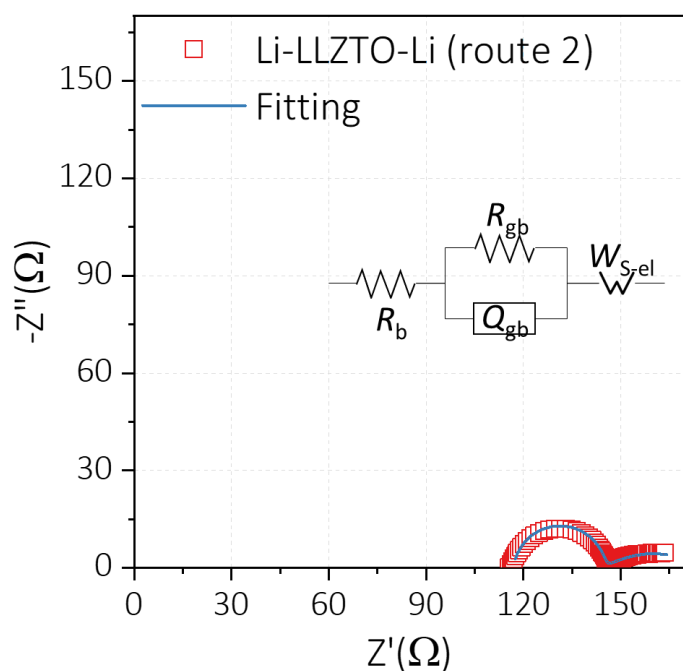


Figure S10 Nyquist plots for EIS spectra of the Li/LLZTO/Li via route 2. Inset shows equivalent circuit used for modeling the EIS data.

As shown in Figure S10 and Figure 4a in the manuscript, it can be found that there was little difference in terms of the Li/LLZTO interface resistance between route 2 and route 4. The interfacial area-specific resistances for route 2 (Figure S10) and route 4 (Figure 4a in the manuscript) are $16.8 \Omega \text{ cm}^2$ and $17.5 \Omega \text{ cm}^2$, respectively. Even though the surface pollution is more severe for the LLZTO polished in air than that polished in glovebox, as shown in Figure S6, the "polishing and spreading" strategy can effectively obtain good Li/LLZTO interface property. This implies that

the impurities on the Li anode play a more important role than the impurities on the LLZTO surface in determining the Li/garnet wettability.

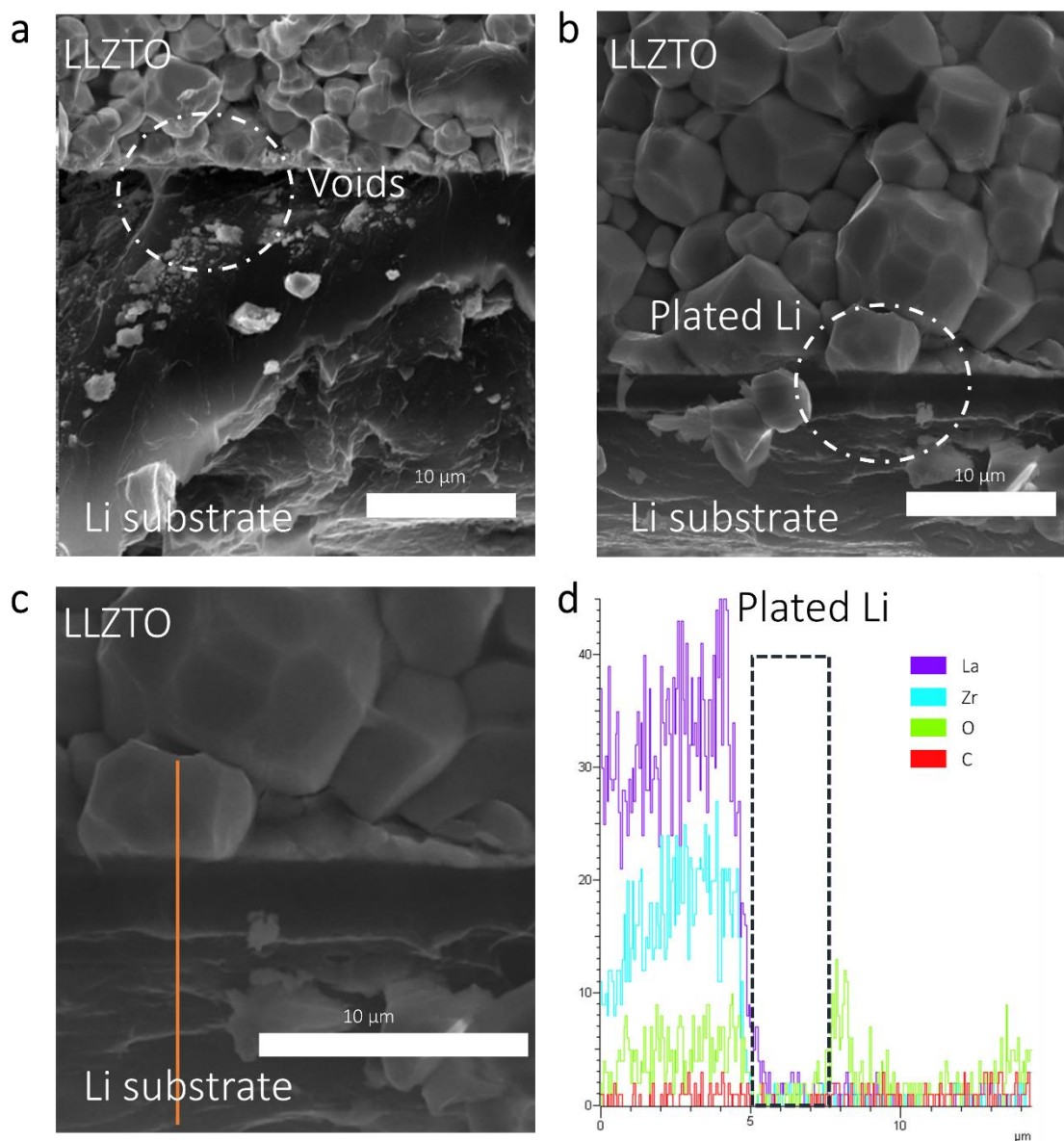


Figure S11 Characterization of the Li/LLZTO interface after cycling, SEM for the stripping side (a) and plating side (b,c), and the element distribution analysis corresponding to the orange line in Figure c.

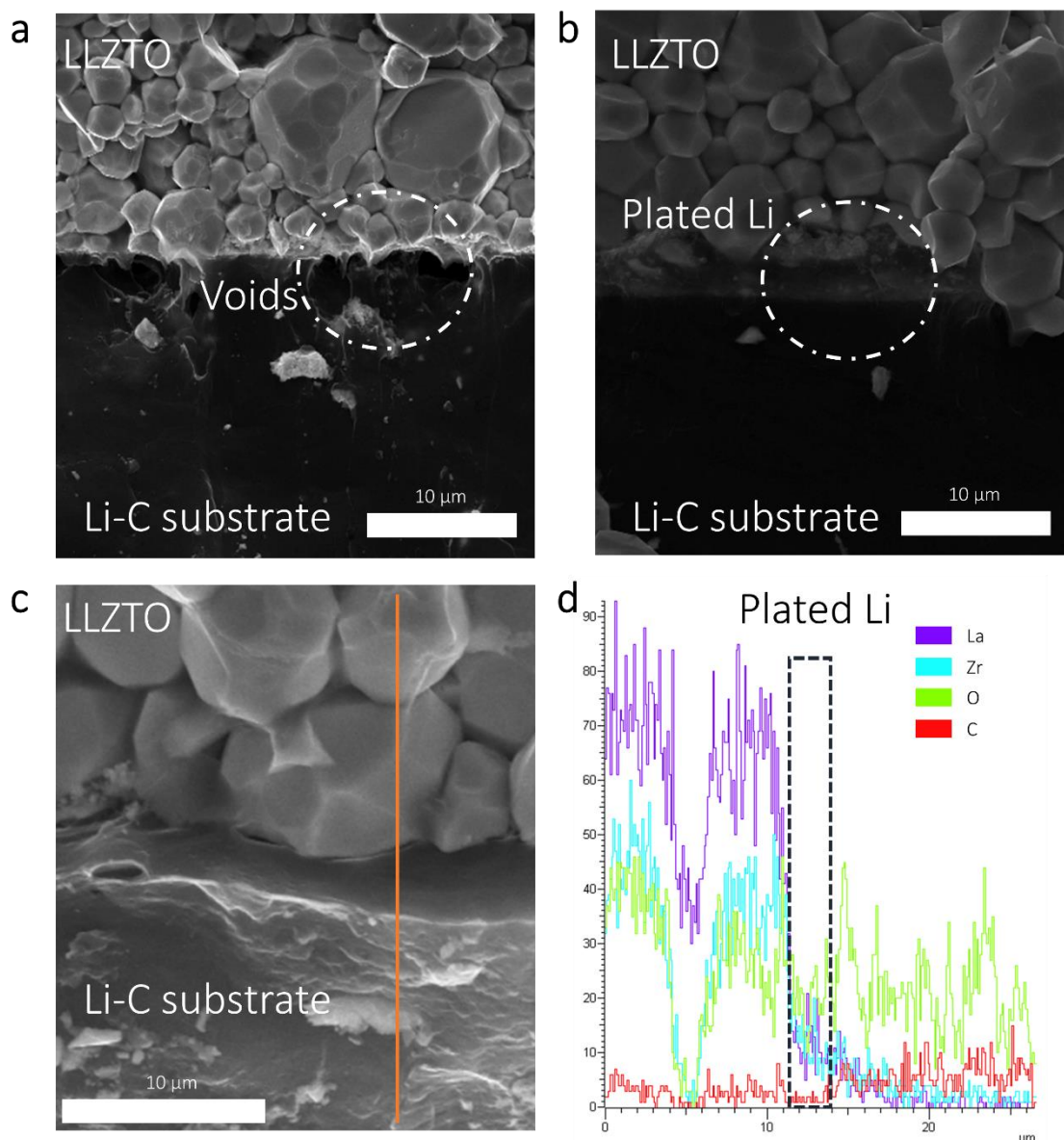


Figure S12 Characterization of the Li-C/LLZTO interface after cycling, SEM for the stripping side (a) and plating side (b,c), and the element distribution analysis corresponding to the orange line in Figure c.

Figure S11a and S12a show that on the stripping side, voids are present in the lithium electrode as a result of insufficient mass transport of lithium atom, causing the polarization increase. Figure S11b and S12b show that on the plating side, a $\sim 2.5 \mu\text{m}$ thick lithium layer forms between the anode and LLZTO, which corresponds to the plating capacity of 0.5 mAh cm^{-2} . It is noted from Figure S12c-d that the plated

lithium has little carbon content by the element distribution analysis, which implies that the plated lithium is pure lithium rather than Li-C.

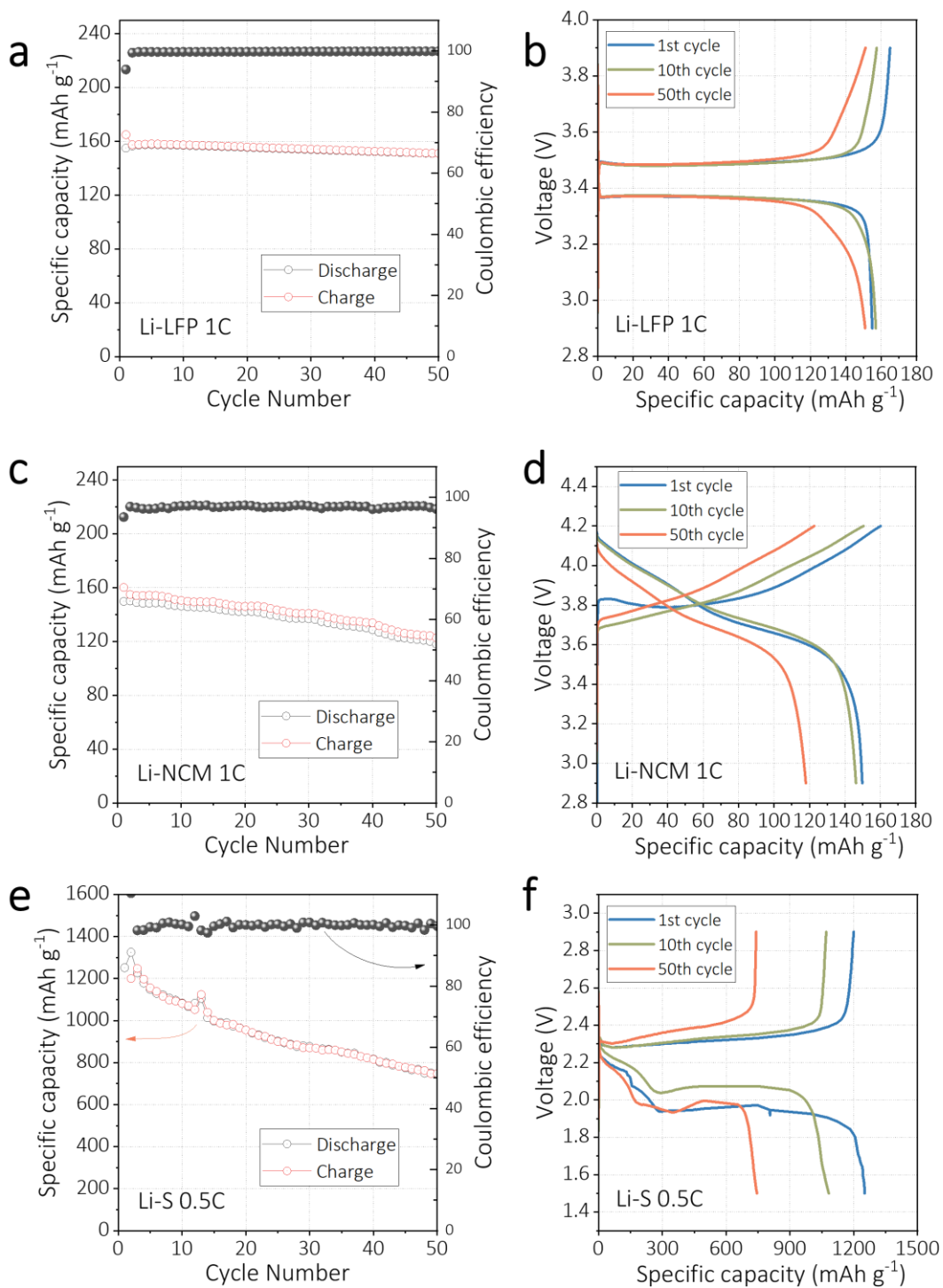


Figure S13 Electrochemical performance of the cell assembled with the Li/LLZTO stack via the "polishing-and-spreading" strategy. Cycling performance of Li/LLZTO/LFP (a), Li/LLZTO/NMC (c) and Li/LLZTO/S (e) for 50 cycles at room temperature. Voltage profiles of Li/LLZTO/LFP (b), Li/LLZTO/NMC (d), and Li/LLZTO/S (f) at the 1st, 10th and 50th cycles.

Table S1 Shear modulus, bulk modulus, and mismatch of Li₂CO₃, LiF, LiOH, Li, LiC₆, and Li₂O with LLZTO in the interface models.

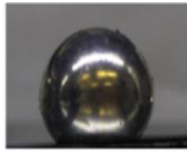
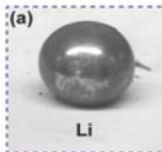

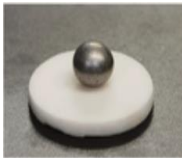
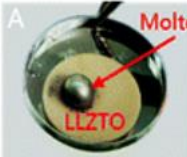
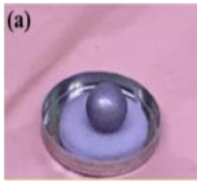
Interface Type (LLZTO-X)	Shear Modulus GV (Gpa)	Bulk Modulus KV (Gpa)	Mismatch (%)
LLZTO-Li ₂ CO ₃	32	63	0.69
LLZTO-LiF	52	70	6.28
LLZTO-LiOH	16	18	9.92
LLZTO-Li	6	14	5.68
LLZTO-LiC ₆	198	242	13.59
LLZTO-Li ₂ O	71	78	1.78

Table S2 Parameters for the Rietveld refinement for Li_{6.5}La₃Zr_{1.5}Ta_{0.5}O₁₂ at 298 K using X-ray diffraction data. R-factors were R_p=5.65%, R_{wp}=7.43%, R_{exp}=4.97% and $\chi^2=2.24\%$.

Atom	site	x	y	z	B	Occupancy
La	24c	0.125	0	0.250	0.425	0.25
Zr	16a	0	0	0	0.296	0.126
Ta	16a	0	0	0	0.296	0.041
Li1	24d	0.250	0.857	0	0.500	0.250
Li2	96h	0.035	0.656	0.549	0.500	1.000

O	96h	0.280	0.107	0.192	0.279	1.000
---	-----	-------	-------	-------	-------	-------

Table S3 Comparison of the Li/LLZO wettability with the literature

Molten Lithium surface	Colour of Lithium surface	ASR ($\Omega \text{ cm}^2$)	Wettability result	Method	Reference
	Dark greyish	\	Lithiophobicity	Heating Or coating	[8]
	Dark greyish	1100	Lithiophobicity	LiSn alloy	[9]
	Dark greyish	661	Lithiophobicity	Ag-Coated	[10]
	Dark greyish	\	Lithiophobicity	Sb-Coated	[11]
	Dark greyish	1126	Lithiophobicity	Li3PO4 modification layer.	[12]
	Dark greyish	4351.6	Lithiophobicity	Graphite layer	[13]

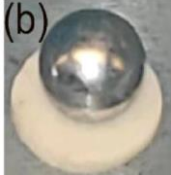
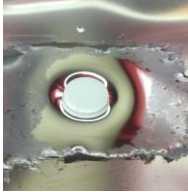
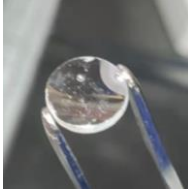
	Dark greyish	675	Lithiophobicity	CF layer	[14]
	Shining metallic	17.5	lithiophilicity	Without any layer and alloying	This work
	Li				

Table S4 Electrode information, test conditions and the electrochemical results for Li/LLZTO/LFP, Li/LLZTO/NMC, and Li/LLZTO/S with the Li/LLZTO stack using the "polishing-and-spreading" strategy.

Cathode	Loading (mg cm ⁻²)	Charge/discharge Rate	Current density (mA cm ⁻²)	Discharge capacity for 1st cycle (mAh g ⁻¹)	Discharge capacity for 10th cycle (mAh g ⁻¹)	Discharge capacity for 50th cycle (mAh g ⁻¹)
LFP	3.0	1C	0.51	155.0	157.0	150.9
NMC	2.5	1C	0.45	149.8	146.3	118.0
Sulfur	0.5	0.5C	0.419	1251.3	1083.8	744.9

Supplementary References:

- [1] G. Kresse, J. Furthmüller, *Physical Review B* **1996**, 54, 11169.
- [2] J. P. Perdew, M. Ernzerhof, K. Burke, *The Journal of Chemical Physics* **1996**, 105, 9982.
- [3] H. J. Monkhorst, J. D. Pack, *Physical Review B* **1976**, 13, 5188.
- [4] a) Z. Liu, Y. Qi, Y. X. Lin, L. Chen, P. Lu, L. Q. Chen, *J. Electrochem. Soc.* **2016**, 163, A592; b) J.-F. Wu, B.-W. Pu, D. Wang, S.-Q. Shi, N. Zhao, X. Guo, X. Guo, *ACS Appl. Mater. Interfaces* **2019**, 11, 898; c) L. Pastero, F. R. Massaro, D. Aquilano, *Crystal Growth & Design* **2007**, 7, 2749; d) M. Bruno, M. Prencipe, *Surf. Sci.* **2007**, 601, 3012; e) K. Leung, *Physical Chemistry Chemical Physics* **2020**, 22, 10412.

- [5] H. Zheng, S. Wu, R. Tian, Z. Xu, H. Zhu, H. Duan, H. Liu, *Adv. Funct. Mater.* **2020**, 30, 1906189.
- [6] L. Zhuang, X. Huang, Y. Lu, J. Tang, Y. Zhou, X. Ao, Y. Yang, B. Tian, *Ceram. Int.* **2021**, 47, 22768.
- [7] H. Zheng, G. Li, J. Liu, S. Wu, X. Zhang, Y. Wu, H. Zhu, X. Huang, H. Liu, H. Duan, *Energy Storage Mater.* **2022**, 49, 278.
- [8] J. Wang, H. Wang, J. Xie, A. Yang, A. Pei, C.-L. Wu, F. Shi, Y. Liu, D. Lin, Y. Gong, Y. Cui, *Energy Storage Mater.* **2018**, 14, 345.
- [9] C. Wang, H. Xie, L. Zhang, Y. Gong, G. Pastel, J. Dai, B. Liu, E. D. Wachsman, L. Hu, *Adv. Energy Mater.* **2018**, 8, 1701963.
- [10] X. Xiang, Y. Zhang, H. Wang, C. Wei, F. Chen, Q. Shen, *J. Electrochem. Soc.* **2021**, 168, 060515.
- [11] R. Dubey, J. Sastre, C. Cancellieri, F. Okur, A. Forster, L. Pompizii, A. Priebe, Y. E. Romanyuk, L. P. H. Jeurgens, M. V. Kovalenko, K. V. Kravchyk, *Adv. Energy Mater.* **2021**, 11, 2102086.
- [12] Y. Ruan, Y. Lu, X. Huang, J. Su, C. Sun, J. Jin, Z. Wen, *J. Mater. Chem. A* **2019**, 7, 14565.
- [13] C. Cui, Q. Ye, C. Zeng, S. Wang, X. Xu, T. Zhai, H. Li, *Energy Storage Mater.* **2022**, 45, 814.
- [14] G. Yang, Y. Zhang, Z. Guo, C. Zhao, X. Bai, L. Fan, N. Zhang, *Electrochim. Acta* **2022**, 407, 139767.